Edge detection based on human visual response

MALAY K. KUNDU† and SANKAR K. PAL†

An algorithm based on the characteristics of the human visual system is presented by which it is possible to select automatically (without human intervention) the thresholds for detecting the significant edges as perceived by human beings. The threshold value changes with the background intensity according to the criterion governed by the characteristic of one of the De Vries–Rose, Weber, and saturated regions. The effect of background size and splitting image (dynamic thresholding), and a provision for reducing the computation time are also included in the study. The algorithm is found to provide a satisfactory improvement in the performance over the conventional edge detection process for a wide range of input image.

1. Introduction

Visual information is concentrated at points of large spatial variation of light intensity in a picture. The difference operators such as gradient, Robert gradient, Sobel and Prewitt gradients, and laplacian (Gonzalez and Wintz 1977) give rise to high values at the places where the change in grey-level occurs. The greater the spatial variation of intensity, the easier is the detection of change and the stronger is the edge intensity. Thresholding of the spatial difference of greylevels (gradient image) is one of the popular techniques for sharpening the edges (i.e. selecting valid or significant edge points according to human perception—Buchsbaum 1980, Brown and Deffenbacher 1979, Nevatia 1982). The problem of edge detection therefore boils down to finding out an appropriate threshold which may be global, local, or dynamic such that if the spatial difference at a point exceeds that threshold, then and only then will it be considered as a valid edge point.

The present work is an attempt to make this task automatic by providing an adaptive algorithm based on human psycho-visual phenomena. The visual increment threshold curve (Buchsbaum 1980) is piecewise linearly approximated here such that the spatial difference in grey-level at a point is thresholded depending on its background intensity by one of the criteria in the De Vries-Rose, Weber and saturated regions.

The algorithm has two stages. In the first stage, grey tone edges are extracted using any spatial difference operator. The elimination of the undesirable edges based on the human visual response (Buchsbaum 1980) is the task of the second stage.

Besides these, the investigation in this paper also comprises the following:

(a) studying the effect of a different background size on the edge-detected output;

(b) splitting the image in order to investigate the effect of dynamic thresholding (Wezka 1978) on edge detection;

(c) proposing a new special difference operators embedded into the thresholding

---

process (second stage) to avoid the additional computation in stage one.

The robustness of the algorithms is demonstrated for various images having unimodal, bimodal, multimodal, and a flat-wide valleyed histogram, and the performances are compared with the standard thresholding technique.

2. Edge operators and thresholding

Let x_{mn} be the grey-level of the (m, n)th pixel of an $M \times N$-dimensional, L-level image $X = [x_{mn}]$, for $m = 1, 2, ..., M; n = 1, 2, ..., N$. The gradient x'_{mn} denoting the edge intensity at the point (m, n) may be defined as (Hall 1979)

$$x'_{mn} = \frac{(|G_1| + |G_2|)}{2} \tag{1}$$

where G_1 and G_2 are given by (2), (3) and (4) corresponding to the ordinary gradient, the Robert gradient, and the Prewitt and Sobel gradients.

$$G_1 = x_{mn} - x_{m,n+1} \tag{2 a}$$

$$G_2 = x_{mn} - x_{m+1,n} \tag{2 b}$$

$$G_1 = x_{mn} - x_{m+1,n+1} \tag{3 a}$$

$$G_2 = x_{m,n+1} - x_{m+1,n} \tag{3 b}$$

$$G_1 = \frac{1}{2+W}[(x_{m+1,n+1} + Wx_{m+1,n} + x_{m+1,n-1})$$
$$- (x_{m-1,n+1} + Wx_{m-1,n} + x_{m-1,n-1})] \tag{4 a}$$

$$G_2 = \frac{1}{2+W}[(x_{m-1,n+1} + Wx_{m,n+1} + x_{m+1,n+1})$$
$$- (x_{m+1,n-1} + Wx_{m,n-1} + x_{m-1,n-1})] \tag{4 b}$$

with $W = 1$ and 2 for the Prewitt and Sobel gradients respectively. These are called the first difference operators. The second difference operator such as the laplacian can be expressed as

$$G_1 = \frac{1}{2}(x_{m-1,n} + x_{m+1,n} - 2x_{mn}) \tag{5 a}$$

$$G_2 = \frac{1}{2}(x_{m,n-1} + x_{m,n+1} - 2x_{mn}) \tag{5 b}$$

The simple gradient and the Robert gradient—(2) and (3)—not only respond strongly to the edges but also to the isolated points. The laplacian does respond to the edges, but it responds more strongly to the corners, lines, line ends, and isolated points. It has a zero response to a linear ramp but it responds strongly where there is a change in the rate of change of the grey-level. Due to some smoothing effect, the Prewitt and Sobel operators, on the other hand, possess a better noise immunity and a good edge response; added to this, the weighted average in the Sobel operator—(4) with $W = 2$—reduces to a great extent the blurring effect of smoothing.

There are other techniques such as (Pal and Majumder 1986)

$$x'_{mn} = \max_{Q}(x_{ij}) - \min_{Q}(x_{ij})$$

where Q is the set of pels in the 3×3 neighbourhood which measures the spatial

difference using the connective property such that edges can also be detected. Based on the above concept, let us formulate two edge-detection methods using contrast, instead of intensity, as a parameter of measurement.

Let ΔC_1 and ΔC_2 denote the contrast of an object pel with respect to its average background intensity and the average contrast within the background itself respectively, such that

$$\Delta C_1 = x_{mn} - \frac{1}{2}\left[\frac{1}{4}\sum_{Q_1} x_{ij} + \frac{1}{2^{5/2}}\sum_{Q_1'} x_{kl}\right] \tag{5 c}$$

$$(i,j) \in Q_1, \quad (k,l) \in Q_l'$$

$$\Delta C_2 = \left|\frac{1}{4}\sum_{Q_l} x_{ij} - \frac{1}{2^{5/2}}\sum_{Q_l'} x_{kl}\right| \tag{5 d}$$

where Q_l and Q_l' are the sets of neighbouring pels with distance 1 and $2^{1/2}$ respectively. Then x_{mn}' can be defined as

$$x_{mn}' = \max |(\Delta C_1 - \Delta C_2), 0| \tag{5 e}$$

In the second method x_{mn}' is defined as

$$x_{mn}' = \max\left(\left|x_{mn} - \max_Q (x_{ij})\right|, \left|x_{mn} - \min_Q (x_{ij})\right|\right)$$
$$- \left[\max_Q (x_{ij}) - \min_Q (x_{ij})\right] \tag{5 f}$$

The definitions (5 e) and (5 f) give rise to some positive results only when the contrast of the object with respect to the background is significant.

After applying these operators on an image X, an edge is deemed to be present at the point (m, n) if x_{mn}' exceeds a predefined threshold value T. The general form of T is

$$T = f(x_{mn}, N_{mn}, (m, n)) \tag{6}$$

where N_{mn} denotes some local property at the point (m, n) having a pixel intensity x_{mn}.

The threshold is called 'global' if T depends only on x_{mn}. When T depends on both x_{mn} and N_{mn}, it is called 'local'. If T depends on the coordinate (m, n) in addition to x_{mn} and N_{mn}, the threshold so computed is defined as 'dynamic'. A good review on different thresholding techniques has been given by Wezka (1978). The selection of an appropriate threshold therefore poses an important problem in detecting the valid edge points in X.

In the following sections, we are going to present an automatic threshold selection procedure based on human psycho-visual facts. The selection is made on the basis of both local and global information available from X such that for a particular x_{mn}' its threshold value adapts with its average background intensity B_{mn} following either $K_2(B_{mn})^{1/2}$ in the De Vries–Rose region, $K_1 B_{mn}$ in the Weber region, or $K_3 B_{mn}^2$ in the saturation region (K_1, K_2 and K_3 being positive constants).

3. Human psycho-visual phenomena

Brightness is a psychological sensation associated with the amount of light stimulus. Owing to the great adaptive ability of the eye, absolute brightness cannot be measured by a human eye. The relative brightness is an observer's feeling of difference

in greyness between the objects. The term contrast is used to emphasize the difference in illuminance of objects. The perceived greyness of a surface depends on its local background and the perceived contrast remains constant if the ratios of contrasts between the object and local background remain constant (Hall 1979).

In psychophysiology, the perceived contrast C refers to the ratio of the difference in luminance of an object B_0 and its immediate surrounding B_S, i.e.

$$C = \frac{|B_0 - B_S|}{B_S} = \frac{\Delta B}{B_S} \tag{7}$$

The visual increment threshold (or the just noticeable difference) is defined as the amount of light ΔB_T necessary to add to a visual field of intensity B such that it can be discriminated from a reference field of the same intensity B. It therefore gives a limit for a perceiveable change in luminance or intensity.

The major problems at low intensity level which any image processing system has to face are as follows (Nevatia 1982):

(a) detection of changes occurring in a low steady but visible illumination (i.e. minimum detectable change); and

(b) detection of the mere presence or absence of light under dark adapted condition (i.e. absolute visual threshold).

At low intensity near the absolute visual threshold, the visual increment threshold ΔB_T is constant. With increases in intensity B, ΔB_T converges asymptotically to the Weber behaviour, i.e. $\Delta B_T \propto B$. This type of behaviour is exhibited in the brightness incremental threshold for white broad band spectra and monochromatic narrow band spectra (Buchsbaum 1980).

Figure 1 presents such a characteristic response in the $\log \Delta B_T - \log B$ plane. *Weber* behaviour is characterized by a unit slope of the curve. The preceding region with slope 1/2 is known as the *De Vries–Rose region*. It has been shown (Buchsbaum 1980) that if the centre visual processor behaves as an optimum probabilistic detector, the incremental visual threshold follows the square-root law, i.e. $\Delta B_T \propto (B)^{1/2}$.
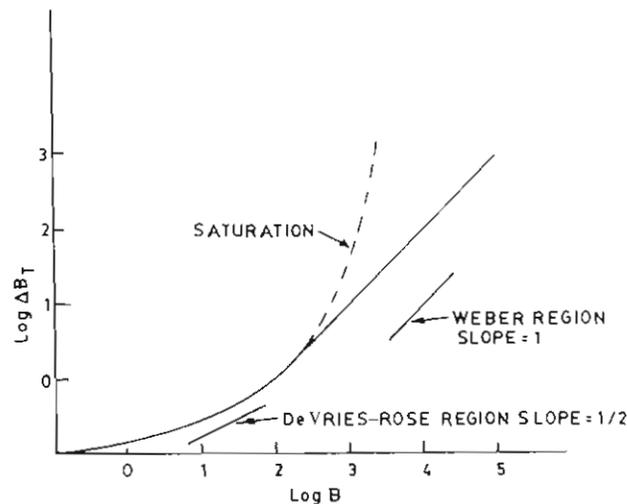

Figure 1. Increment threshold ΔB_T as a function of reference intensity B.

However, in an actual case this rule is followed in a small restricted region (Fig. 1). The dashed curve shows the deviation from the Weber law. This deviation (which represents a *saturation region*) is not usually exhibited by the retinal cone mechanism even under very high intensities but could happen in very restricted cases.

From Fig. 1 it is seen that the variation of $\log \Delta B_T$ against $\log B$ in the De Vries–Rose region is slower than that in the Weber region. In other words, the discrimination ability in the De Vries–Rose region is greater than in the Weber region. The possible reason for this deterioration in discrimination ability can be attributed to visual non-linearity.

Assuming the response curve (Fig. 1) to be piecewise linear, the Weber region and the De Vries–Rose region can be represented as

$$\log \Delta B_T = \log (K_1 B) = \log B + \log K_1 \tag{8}$$

and

$$\log \Delta B_T = \log (K_2 (B)^{1/2}) = \tfrac{1}{2} \log B + \log K_2 \tag{9}$$

respectively. Here K_1 and K_2 are the constants of proportionality.

Furthermore, the saturation which might occur even rarely, only at very high intensities can be approximated as

$$\log \Delta B_T = 2 \log B + \log K_3 \tag{10}$$

K_3 being a constant.

Therefore, when the brightness value of an object is higher (or lower) than its surrounding, background, or reference intensity B by an amount $\geqslant \Delta B_T$, it corresponds to a point on or above the curve (Fig. 1), and the object will appear either brighter (or darker). In case of a variable object and background intensity, the visual system adapts to an average intensity.

Furthermore, Fig. 2 shows the variation of $\Delta B_T/B$ with B. It is seen that in the Weber region, the ratio $\Delta B_T/B$ remains fairly constant at about β % of its maximum value over a very wide range of its B-value. In the literature the value of β is said to be around 0·02.
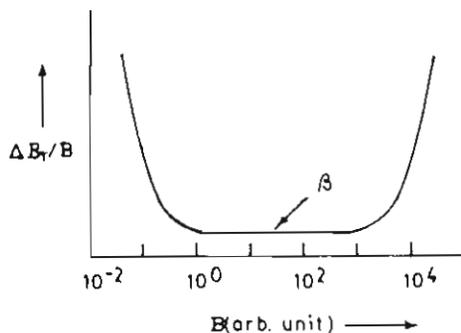

Figure 2. Variation of contrast sensitivity $\Delta B_T/B$ with background intensity B for uniform background.

It is also mentioned in the literature (Zuidema 1983) that the threshold value is highly dependent on the size of the background. As the background size increases the threshold value also increases; this variation continues up to some maximum size of the background beyond which it becomes independent of the background size. This

indicates that a larger value of ΔB_T will be required for the values of B computed over a larger background or window size. So it is expected that as the size of the background increases a smaller number of edge points will be detected by the visual system.

4. Adaptive threshold selection

The piecewise linear approximation of the visual increment threshold curve (Fig. 1) is shown in Fig. 3. Here, the threshold values in the De Vries–Rose region, the Weber region, and the saturation region are defined by the linear equations (8), (9) and (10) respectively. Although the demarcation between these regions represented by various equations is not very sharp and definite, we assume here for the sake of simplicity and ease of analysis that the De Vries–Rose region extends between x_1 and x_2—Fig. 3—(x_1 corresponds to the absolute visual threshold), the Weber region between x_2 and x_3, and the saturation region beyond x_3. The value of B corresponding to $\log B = x_i$ is assumed here to be B_{x_i}, for $i = 1, 2, 3$. In other words
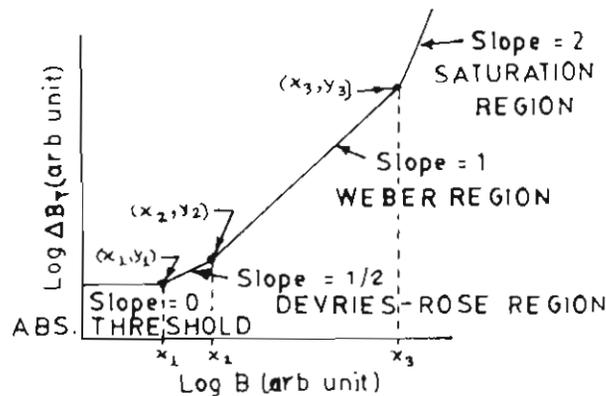
$$x_i = \log B_{x_i}, \quad i = 1, 2, 3 \tag{11}$$

Figure 3. Increment threshold ΔB_T vs reference intensity B curve (Fig. 1) with linear approximation for different regions.

Let x_0 and B_l be the maximum value of $\log B$ and B, respectively. Let us assume further that

$$x_i = \alpha_i x_0, \quad i = 1, 2, 3 \tag{12}$$

and

$$B_{x_i} = \alpha_i' B_l, \quad i = 1, 2, 3 \tag{13}$$

where

$$0 < \alpha_1 < \alpha_2 < \alpha_3 < 1$$
$$0 < \alpha_1' < \alpha_2' < \alpha_3' < 1$$

As mentioned in § 1, the value of $\Delta B_T/B$ remains fairly constant over the entire Weber region with a value approximately equal to β % of $(\Delta B/B)_{max}$, the maximum value of

$\Delta B/B$ over the entire dynamic range. Therefore, from (8) one can write

$$K_1 = \frac{\Delta B_T}{B} = \frac{1}{100} \beta \left(\frac{\Delta B}{B} \right)_{\text{max}} \tag{14}$$

Now, (8) and (9) are both satisfied at the point (x_2, y_2) of Fig. 3. Therefore, we can write

$$y_2 = x_2 + \log K_1 = \tfrac{1}{2} x_2 + \log K_2$$

or

$$\frac{1}{2} x_2 = \log \left(\frac{K_2}{K_1} \right) \tag{15}$$

Using (11) for $i = 2$

$$\frac{1}{2} \log B_{x_2} = \log \left(\frac{K_2}{K_1} \right)$$

or

$$K_2 = K_1 (B_{x_2})^{1/2} \tag{16}$$

Similarly, considering (8) and (10) at the point (x_3, y_3) we have

$$K_3 = \frac{K_1}{B_{x_3}} \tag{17}$$

The minimum values of the increment threshold are therefore

$$\Delta B_T = K_2 (B)^{1/2} = \frac{(B)^{1/2}}{100} \beta \left(\frac{\Delta B}{B} \right)_{\text{max}} (B_{x_2})^{1/2}; \quad B_{x_2} \geqslant B \geqslant B_{x_1} \tag{18 a}$$

$$= K_1 B = \frac{B}{100} \beta \left(\frac{\Delta B}{B} \right)_{\text{max}}, \quad B_{x_3} \geqslant B \geqslant B_{x_2} \tag{18 b}$$

$$= K_3 B^2 = \frac{B^2}{100} \beta \left(\frac{\Delta B}{B} \right)_{\text{max}} \frac{1}{B_{x_3}}, \quad B \geqslant B_{x_3} \tag{18 c}$$

corresponding to the De Vries–Rose, Weber, and saturation regions. Equation (12) defines the minimum amount of brightness level, in three different regions, by which the intensity of an object must be greater or less than its background intensity B in order to make the object appear brighter or darker (i.e. detectable). In other words, for a particular point in a picture having intensity B_p if we have either

$$\frac{\Delta B}{(B)^{1/2}} \geqslant K_2 \quad \text{when } \alpha'_2 B_t \geqslant B \geqslant \alpha'_1 B_t \tag{19 a}$$

or

$$\frac{\Delta B}{B} \geqslant K_1 \quad \text{when } \alpha'_3 B_t \geqslant B \geqslant \alpha'_2 B_t \tag{19 b}$$

or

$$\frac{\Delta B}{B^2} \geqslant K_3 \quad \text{when } B \geqslant \alpha'_3 B_t \tag{19 c}$$

with

$$\Delta B = |B_P - B| \tag{20}$$

then and only then can it be considered as a detectable edge point having edge intensity ΔB.

5. Computation of B_{mn} and $(\Delta B/B)_{max}$

Figure 4 shows the flow chart for extracting valid edges of an $M \times N$-dimensional, L-level image $X = [x_{mn}]$, for $m = 1, 2, ..., M; n = 1, 2, ..., N$ using the above-mentioned adaptive thresholding scheme.
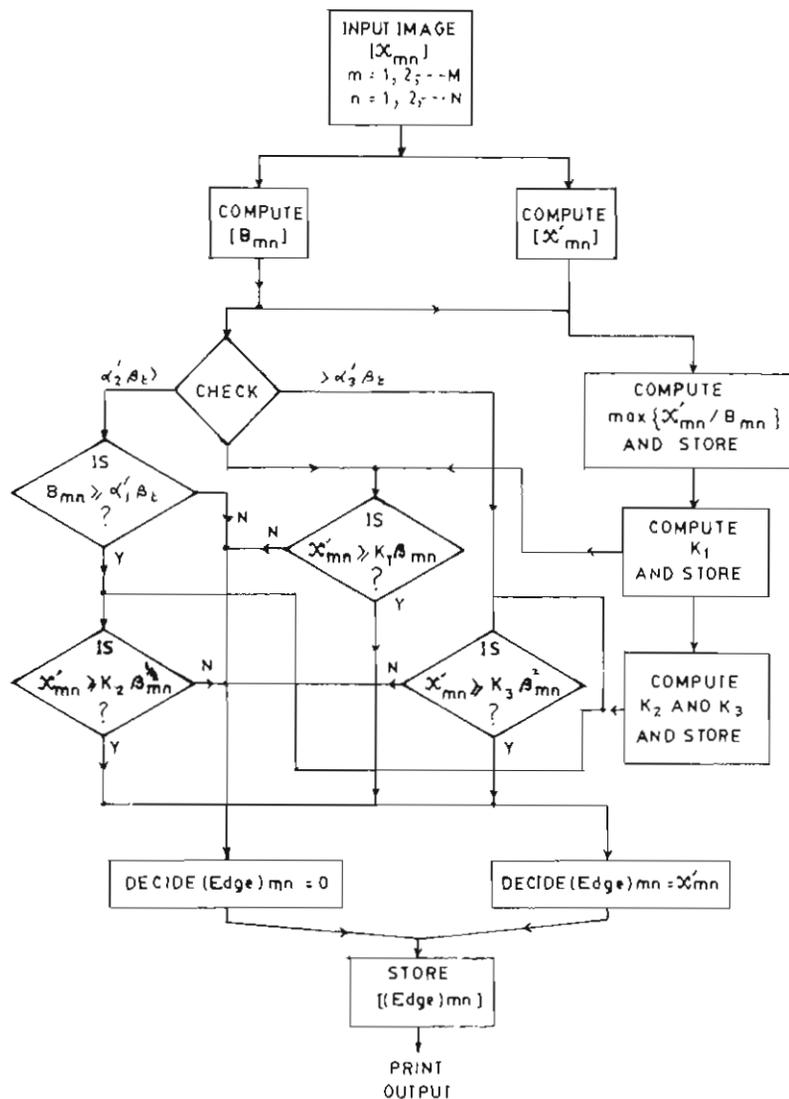

Figure 4. Flow chart for the proposed thresholding algorithm.

Here B_{mn} which denotes the background intensity B at the point (m, n) was considered to be the weighted average over its neighbours. For a 3×3 window size background we consider

$$B_{mn} = \frac{\left\{ \frac{1}{2}\left[\frac{1}{4}\sum_{Q_l} x_{ij} + \frac{1}{4(2)^{1/2}}\sum_{Q_l'} x_{kl} \right] + x_{mn} \right\}}{2}$$

$$(i, j) \in Q_l, \quad (k, l) \in Q_i' \tag{21}$$

where Q_l and Q_l' denote the set of neighbouring pels x_{ij} and x_{kl} which are at a distance of 1 and $(2)^{1/2}$ units, respectively, from x_{mn}.

For a 5×5 size of background

$$B_{mn} = \tfrac{1}{2}(x_{mn} + \tfrac{1}{5}B') \tag{22 a}$$

where

$$B' = \frac{1}{4}\sum_{Q_l} x_{ab} + \frac{1}{4(2)^{1/2}}\sum_{Q_l'} x_{cd} + \frac{1}{8}\sum_{Q_2} x_{ef} + \frac{1}{8(5)^{1/2}}\sum_{Q_2'} x_{gh} + \frac{1}{8(2)^{1/2}}\sum_{Q_2''} x_{ij} \tag{22 b}$$

$$a, b \in Q_l, \quad c, d \in Q_l', \quad e, f \in Q_2$$

$$g, h \in Q_2', \quad i, j \in Q_2''$$

where Q_2, Q_2' and Q_2'' are the sets of pels in the 5×5 neighbourhood of x_{mn} with distances 2 for Q_2, $(5)^{1/2}$ for Q_2', and $2(2)^{1/2}$ for Q_2''.

Similarly, for a 7×7 window size for a background

$$B_{mn} = \tfrac{1}{2}[x_{mn} + \tfrac{1}{9}(B' + B'')] \tag{23 a}$$

where

$$B'' = \frac{1}{12}\sum_{Q_3} x_{kl} + \frac{1}{8(10)^{1/2}}\sum_{Q_3'} x_{pq}$$

$$+ \frac{1}{8(13)^{1/2}}\sum_{Q_3''} x_{rs} + \frac{1}{12(2)^{1/2}}\sum_{Q_3'''} x_{uv} \tag{23 b}$$

$$k, l \in Q_3, \quad p, q \in Q_3'$$

$$r, s \in Q_3'', \quad u, v \in Q_3'''$$

where Q_3, Q_3', Q_3'' and Q_3''' are the sets of pels in the 7×7 neighbourhood of x_{mn} with the corresponding distances 3, $(10)^{1/2}$, $(13)^{1/2}$ and $3(2)^{1/2}$.

Here x_{mn}', denoting the value of ΔB at the (m, n)th point (difference in intensity of x_{mn} with respect to its neighbouring pixels), can be obtained from (1)–(5 b) corresponding to different spatial edge detection (gradient) operators; ΔB can also be calculated from the operators (5 e) and (5 f) using the spatial difference of parameters which are a function of the intensity value of the pels.

It is to be noted here that the individual terms of (21)–(23) representing the average background intensity for different window sizes also appear in (5 c)–(5 f). As a result, no additional computation would be required for computing x_{mn}' when (5 c)–(5 f) are used.

Finally, for computing the constants K_i, for $i = 1, 2, 3$ we consider

$$B_i = \max\,[x_{mn}] - \min\,[x_{mn}] \tag{24}$$

and

$$\left(\frac{\Delta B}{B}\right)_{\text{max}} = \max\left[\frac{x'_{mn}}{B_{mn}}\right] \qquad (25)$$

$m = 1, 2, ..., M$, and $n = 1, 2, ..., N$.

Here, B_t has been taken to be equal to the dynamic range of the input image.

As shown in Fig. 4 the task of thresholding has two stages. In the first stage, each pixel intensity x_{mn} is chosen, on the basis of its local information (namely, background intensity B_{mn}), to satisfy the requirement in one of the three regions. The second stage consists of checking whether x'_{mn} satisfies its respective criterion—(19). If that condition is satisfied, x_{mn} is then treated as a valid edge point having edge intensity x'_{mn}. Otherwise, the edge intensity at the (m, n)th point is taken to be zero. It is to be noted here that the thresholding criterion—(18) or (19)—for a particular x'_{mn} is seen to be adaptive (i.e. changing with its B_{mn} value according to $K_2(B_{mn})^{1/2}$, $K_1 B_{mn}$, or $K_3 B_{mn}^2$ in the respective cases).

Although it was mentioned in § 4 that the threshold value of the Weber region is β % of the $(\Delta B/B)_{\text{max}}$ calculated globally, it is often found, in practice, that due to the imperfection of the acquisition process, the true contrast of the original object is not truly reflected in the captured image. A global type of approach for the computation of $(\Delta B/B)_{\text{max}}$ over the entire image may not be suitable for images having a wide variation of contrast at their different portions. Instead, a semi-global approach (Rosenfeld and Kak 1982), i.e. $(\Delta B/B)_{\text{max}}$ calculated over a smaller segmented block will be desirable. The threshold selection based on this segmented approach may therefore be referred to as 'dynamic' (Wezka 1978).

6. Implementation and results

The algorithm discussed in the previous section was simulated on EC 1033 computer. The output images were generated by an overprinting technique as there is no facility for graphic printing. Some output images were generated with numeric representations of grey-levels due to a printer problem. A set of images having different types of histogram was taken as test data of size 64×64 and with 32 grey-levels. Although it was mentioned in the earlier section that the Weber region covers the major portion of the total dynamic range and both the De Vries–Rose and saturated regions cover a very small portion of it (Buchsbaum 1980), there is no quantitative figure available for the length of span of each region discussed.

Experiments were carried out (Kundu and Pal 1986) for different lengths of span for different regions, namely ($\alpha'_2 = 0.33$, $\alpha'_3 = 0.66$), ($\alpha'_2 = 0.1$, $\alpha'_3 = 0.7$), ($\alpha'_2 = 0.3$, $\alpha'_3 = 0.9$), and ($\alpha'_2 = 0.1$, $\alpha'_3 = 0.9$). It was found that the combination ($\alpha'_2 = 0.1$, $\alpha'_3 = 0.9$) provided the optimum result as far as connectivity and thinness of edges were concerned.

Figures (5)–(9) show the edge-detected output for Biplane, Lincoln, Boy, Jet, and Chromosome images when x'_{mn} was computed with a Robert gradient and B_{mn} was obtained with (21) for the thresholding parameters $\alpha'_2 = 0.1$, $\alpha'_3 = 0.9$ and $\beta = 4.5$. The effect of the variation of β is discussed in our earlier report (Kundu and Pal 1986). Results with other operators such as Sobel and Prewitt are also available in that report.

Figures 5(d), 6(d), ..., 9(d) therefore demonstrate the thresholding version of the gradient images—Figs 5(c), 6(c), ..., 9(c)—using the proposed thresholding algorithm (Fig. 4).
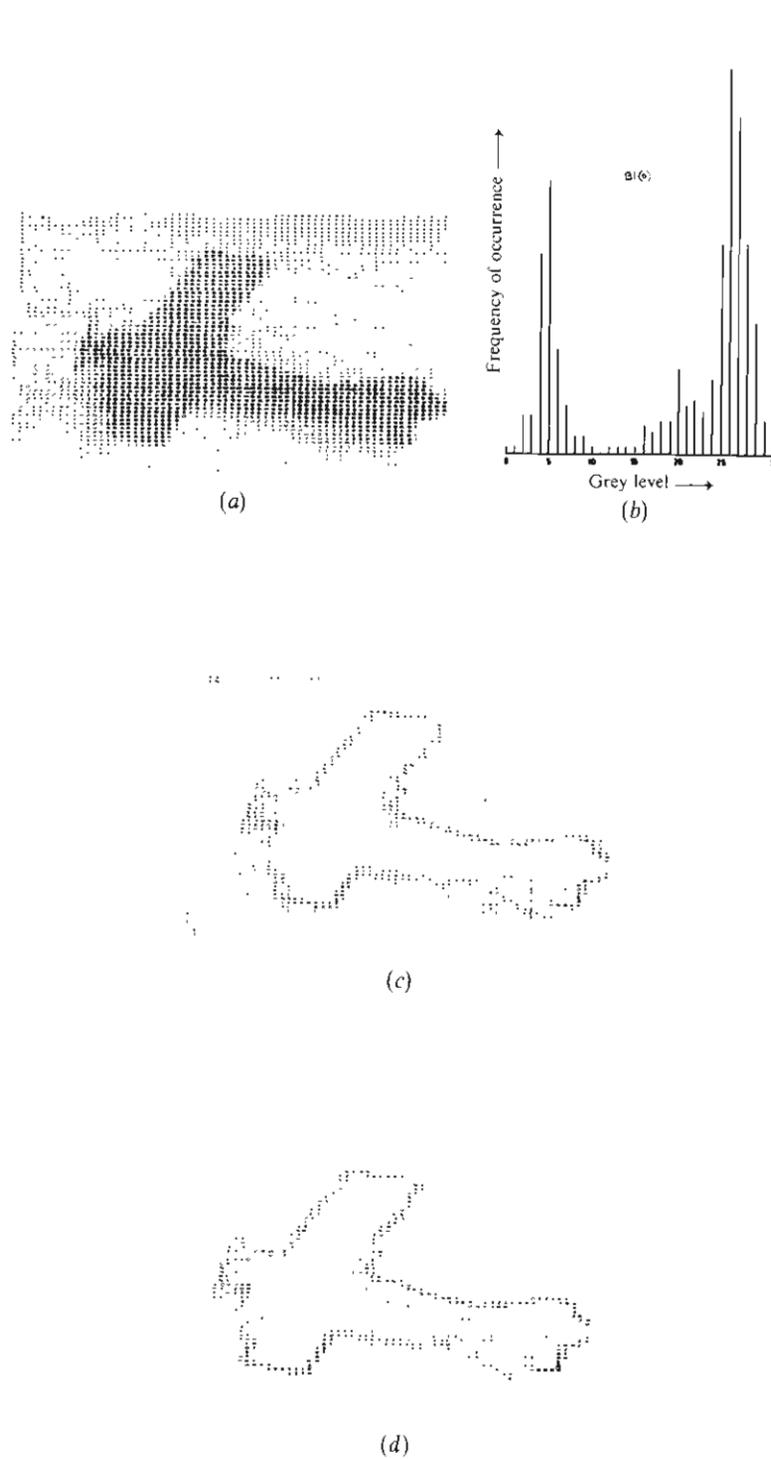
(a)

(b)

(c)

(d)

Figure 5. (a) Input image of Biplane; (b) histogram of the input image; (c) gradient image of Biplane (using Robert gradient); (d) thresholded version of (c) using proposed thresholding algorithm ($\alpha_2' = 0.1$, $\alpha_3' = 0.9$, $\beta = 4.5$).
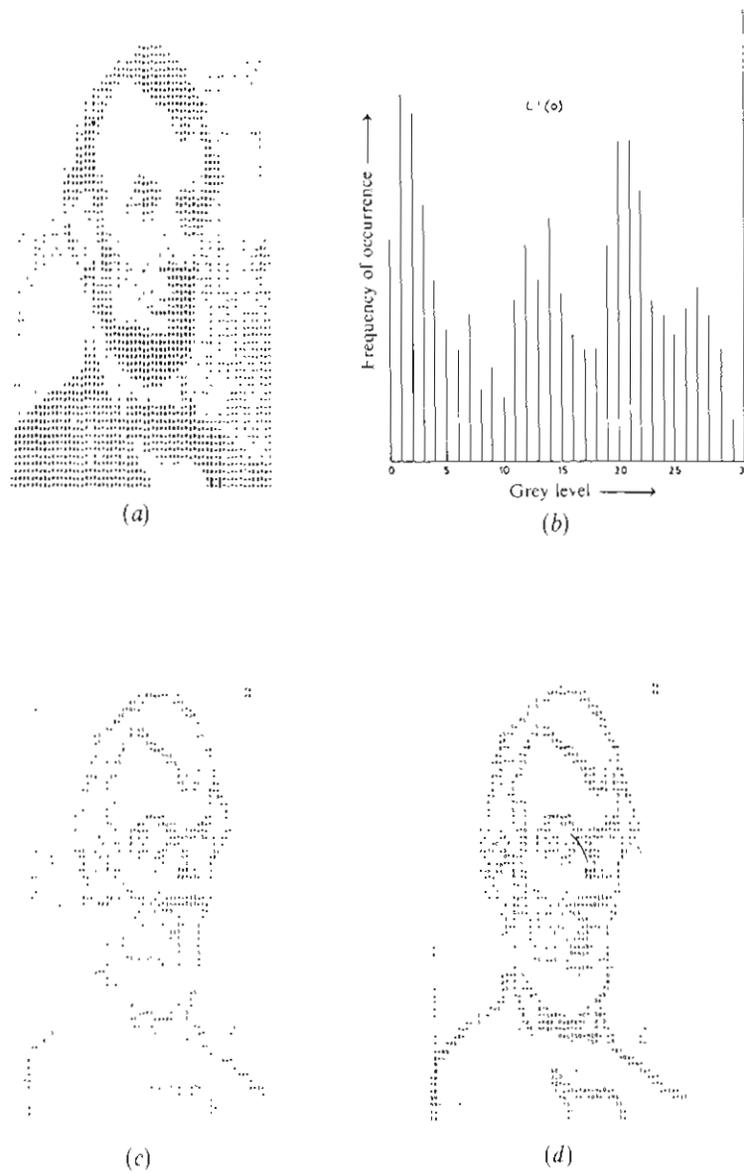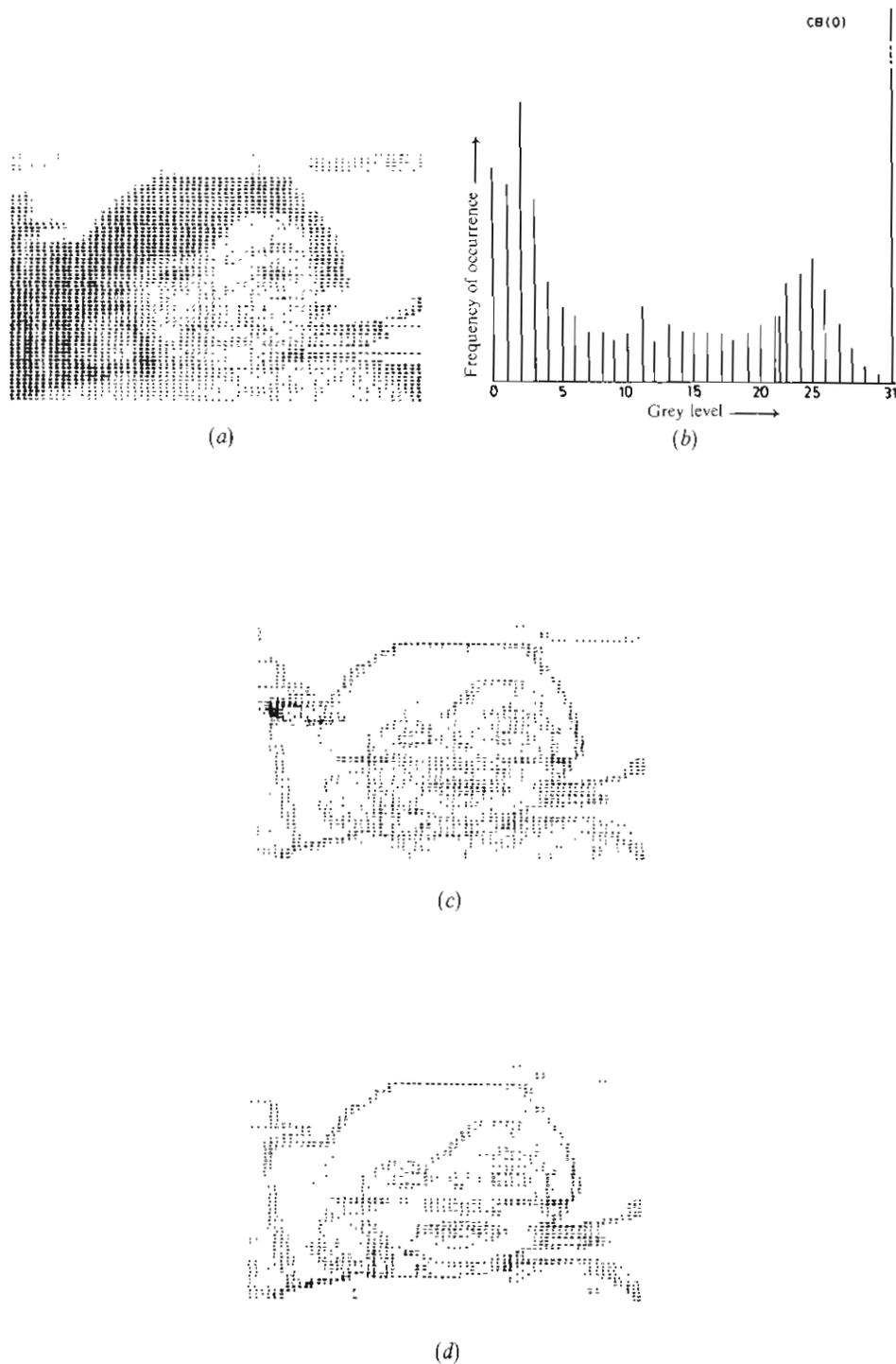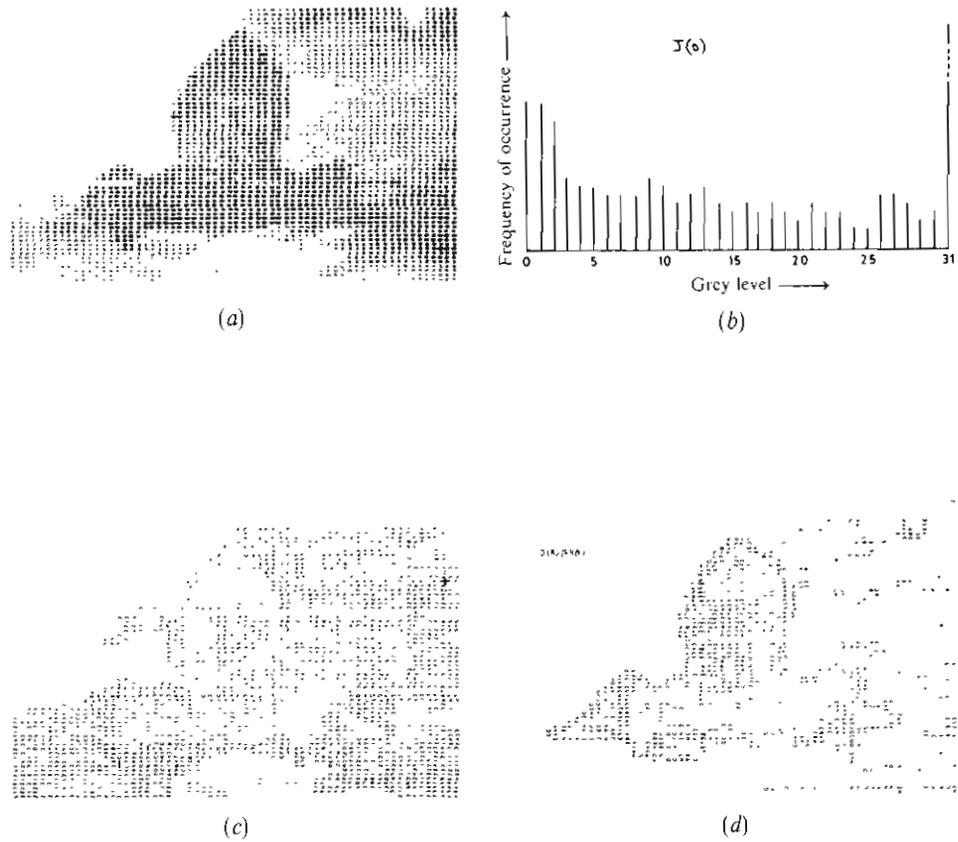
Figure 6.   (a) Input image of Lincoln; (b) histogram of the input image; (c) gradient image of Lincoln (using Robert gradient); (d) thresholded version of (c) using proposed thresholding algorithm ($\alpha'_2 = 0 \cdot 1$, $\alpha'_3 = 0 \cdot 9$, $\beta = 4 \cdot 5$).

(a)

(b)

(c)

(d)

Figure 7. (a) Input image of Boy; (b) histogram of the input image; (c) gradient image of Boy (using Robert gradient); (d) thresholded version of (c) using proposed thresholding algorithm ($\alpha'_2 = 0.1$, $\alpha'_3 = 0.9$, $\beta = 4.5$).
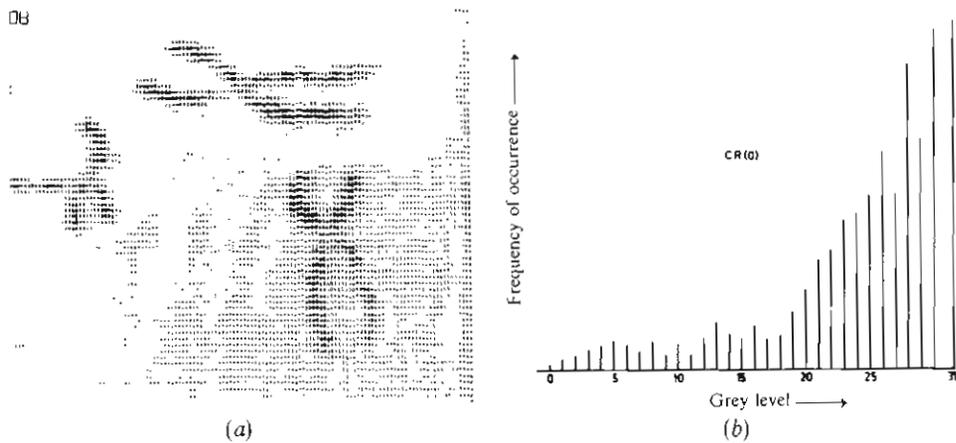
Figure 8. (a) Input image of Jet; (b) histogram of the input image; (c) gradient image of Jet (using Robert gradient); (d) thresholded version of (c) using proposed thresholding algorithms ($\alpha_2' = 0\cdot1$, $\alpha_3' = 0\cdot9$, $\beta = 4\cdot5$).

Figure 9. (a) Input image of Chromosome; (b) histogram of the input image; (c) gradient image of Chromosome (using Robert gradient); (d) thresholded version of (c) using proposed thresholding algorithms ($\alpha'_2 = 0\cdot1$, $\alpha'_3 = 0\cdot9$, $\beta = 4\cdot5$).

Figures 10(a) and 10(b) give the thresholding versions of Fig. 8(c) when this is individually thresholded (Rosenfeld and Kak 1982) at levels 4 and 6. The threshold at 4 could not isolate the jet from the background resulting in undesirable edges. On the other hand, the threshold at 6 made the contour separate out at the cost of disconnecting the right wing. This is shown as an illustration of the improvement of the proposed technique over the conventional one.

Figure 10. (a) Thresholded version of Fig. 8(c) using normal histogram thresholding techniques when thresholded at edge intensity level 4; (b) thresholded version of Fig. 8(c) using the same technique with level of threshold 6.

As discussed in § 5, the results shown in Fig. 11 using (5 e) do not need any additional computation (as in the case of Robert, Sobel etc.) for obtaining the different constituting terms of x'_{mn}. The parameter (α, β, background size) considered here are the same as in Figs (5)–(9). A similar experiment was also conducted for (5 f), but the results are not included here.
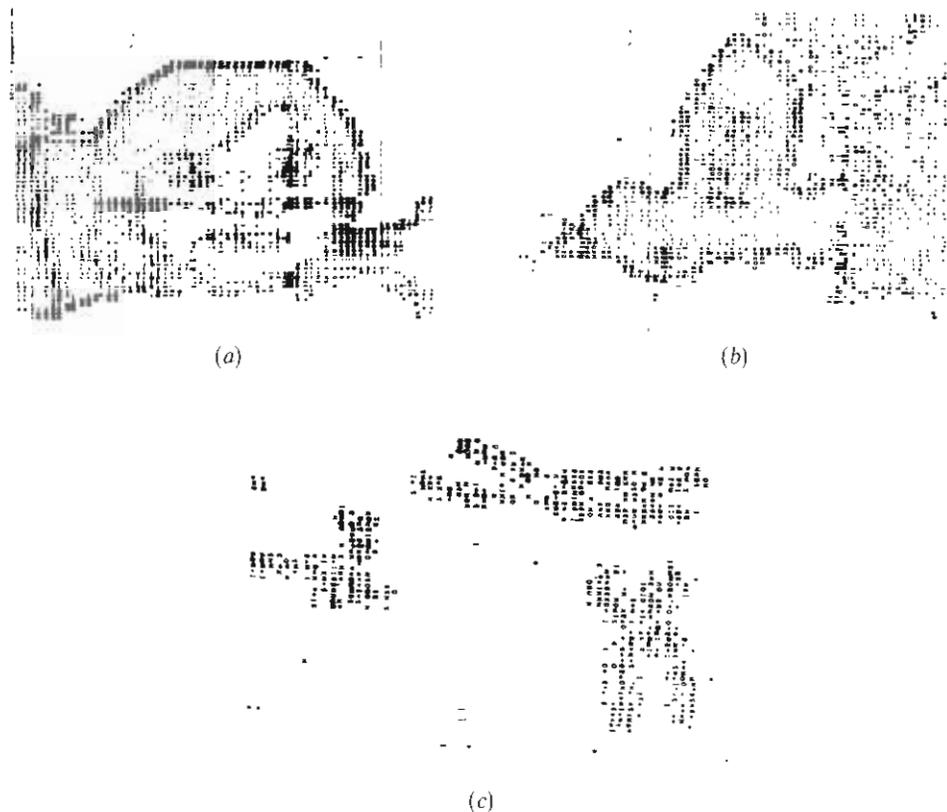
(a)   (b)

(c)

Figure 11. Edge detected version using the new edge operator (5 c) and the proposed thresholding technique with 3×3 background size, $\alpha_2' = 0\cdot1$, $\alpha_3' = 0\cdot9$ and $\beta = 4\cdot5$: (a) for the input image Fig. 7(a); (b) for the input image Fig. 8(a); (c) for the input image Fig. 9(a).

6.1. Effect of background size

It was discussed in §3 that the threshold value is dependent on the size of the background considered for detecting edges. In fact, the threshold value increases with the increase in background size resulting in a smaller number of detectable edge points.

The above fact resembles well the experimental results shown in Figs 12 and 13 corresponding to the Robert gradient and (5 e) when Fig. 7 (a)—Boy—is considered as input with a 5×5 and 7×7 window size (background). Considering Figs 7 (d), 11 (a), 12 and 13 it is seen that as the background size increases from 3×3 to 7×7, the contour becomes thinner. With a further increase in background size, the contours were found to be disconnected.

Some more results in the above context are shown in Fig. 14 for some optimum window sizes.

6.2. Semi-global selection of $(\Delta B/B)_{max}$

The results presented so far are based on the $(\Delta B/B)_{max}$ value obtained over the entire picture (globally). In this section we will be demonstrating the effect of the semi-global selection of that parameter.
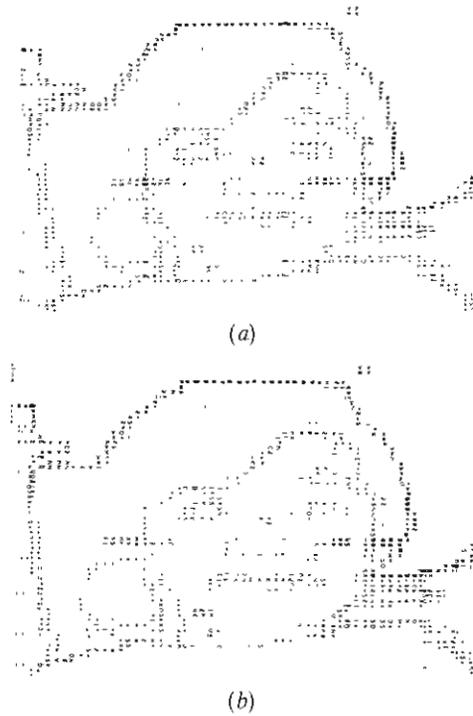
(a)

(b)

Figure 12. Edge-detected version of Fig. 7(a) using the Robert gradient and proposed thresholding technique ($\alpha_2' = 0\cdot1$, $\alpha_3' = 0\cdot9$, $\beta = 4\cdot5$) with: (a) background size = 5×5; (b) background size = 7×7.
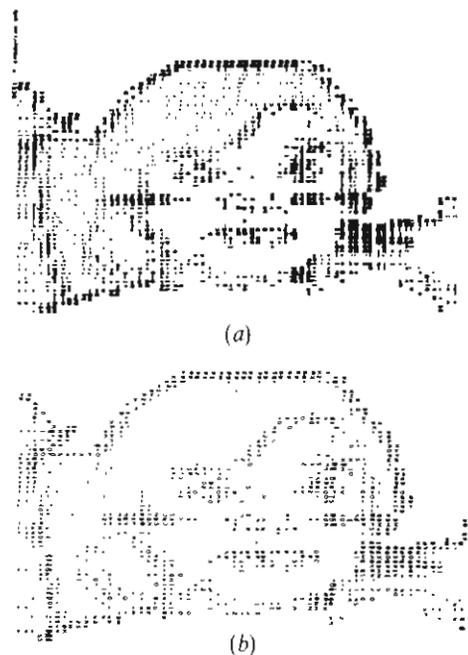

(a)

(b)

Figure 13. Edge-detected version of Fig. 7(a) using new edge operator (5 e) and proposed thresholding technique ($\alpha_2' = 0\cdot1$, $\alpha_3' = 0\cdot9$, $\beta = 4\cdot5$) with: (a) background size = 5×5; (b) background size = 7×7.
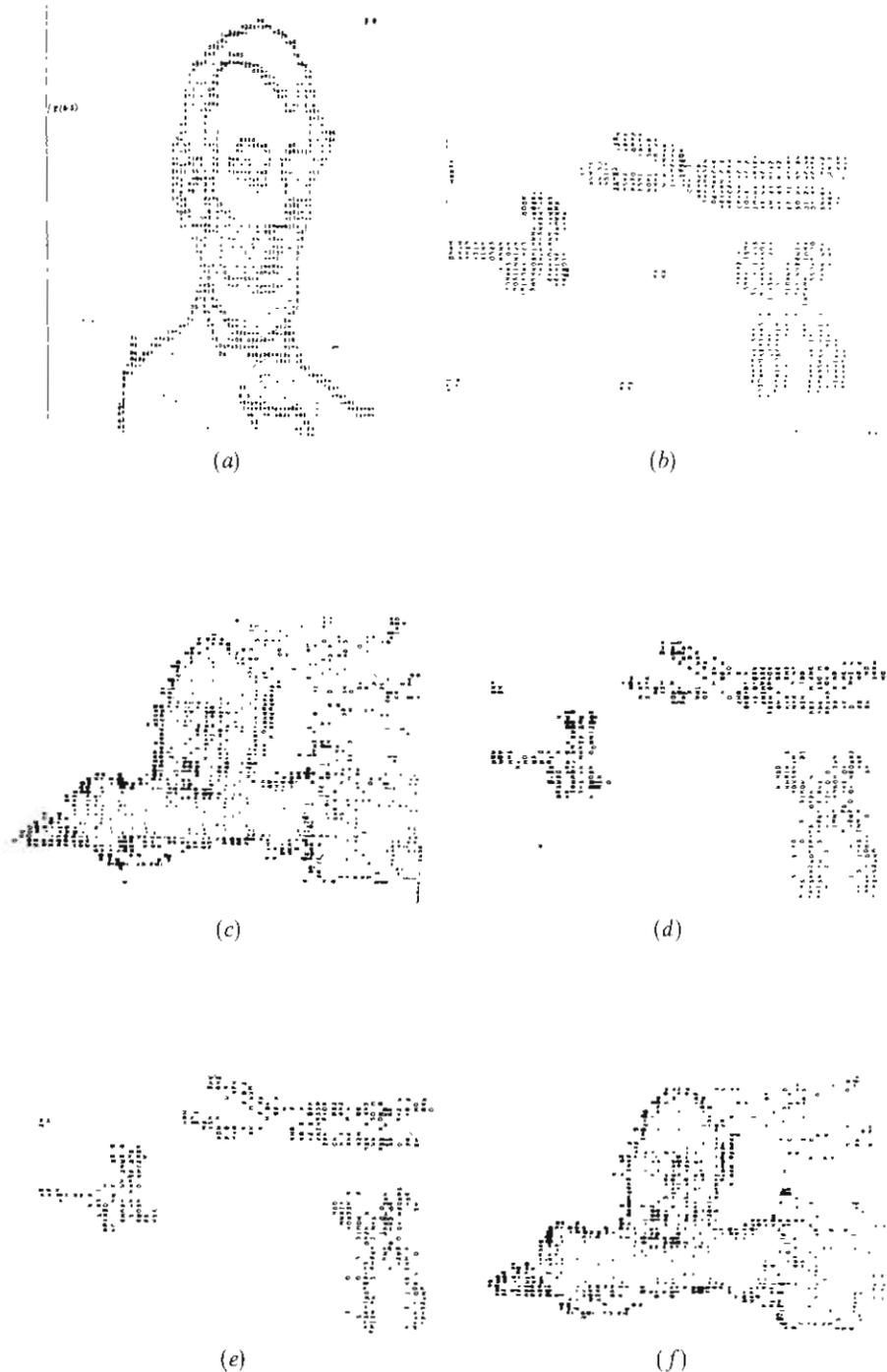
Figure 14.   Edge-detected version using proposed thresholding technique ($\alpha'_2 = 0.1$, $\alpha'_3 = 0.9$, $\beta = 4.5$) for: (a) Fig. 6(a) using the Robert gradient and 5×5 window size (background); (b) Fig. 9(a) same operator and window size as in Fig. 14(a); (c) Fig. 8(a) using new edge operator (5 e) and same window size as in Fig. 14(a); (d) Fig. 9(a) using same operator and window size as in Fig. 14(c); (e) Fig. 8(a) using new edge operator (5 e) and 7×7 window size; (f) Fig. 9(a) using same operator and window size as in Fig. 14(e).

Figure 15 shows the edges of the Jet and Chromosome images using the Robert gradient when the images are divided into four blocks each having dimensions 32 × 32. The $(\Delta B/B)_{max}$ value was computed separately for each block in order to select the thresholds in the respective blocks. The threshold selections have thus become dynamic which enables one to detect more information in the content. Here, the background size, α-values and β-values are the same as in Figs (5)–(9).
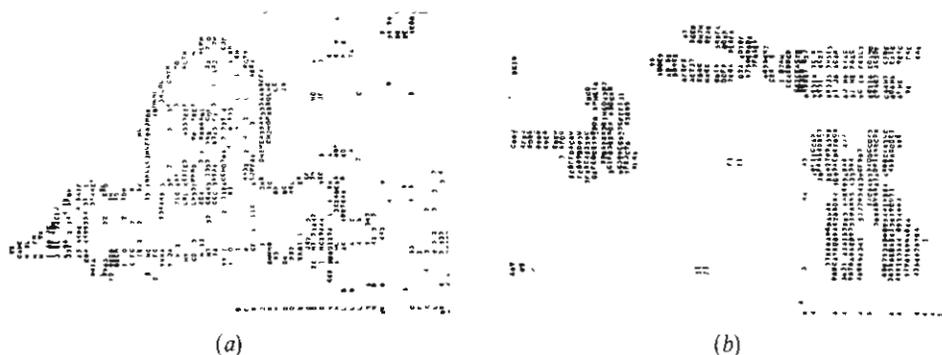

(a) (b)

Figure 15. Edge-detected version using the Robert gradient and the semiglobal selection for the computation of $(\Delta B/B)_{max}$ over window size 32 × 32 for thresholding (with $\alpha'_2 = 0.1$, $\alpha'_3 = 0.9$, $\beta = 4.5$) for: (a) Fig. 8(a); (b) Fig. 9(a).

6.3. *Effect of thresholding on histogram*

To demonstrate the effect of thresholding on the histogram let us consider for example, Fig. 16 (a) which shows the histogram of the Jet image after the Robert gradient is used, and Fig. 16 (b) when it is thresholded adaptively using the proposed thresholding algorithm. Figure 16 (a) shows the frequency of occurrence of probable edge points with different edge intensities. In the normal histogram thresholding
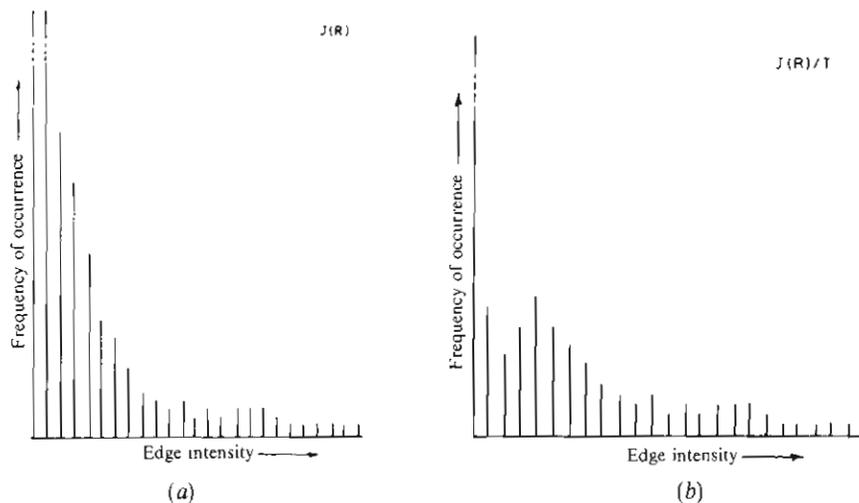

(a) (b)

Figure 16. (a) Histogram of edge intensity (using the Robert gradient) for the Fig. 8(a); (b) histogram of thresholded edge intensity—Fig. 16(a)—using proposed thresholding technique.

technique, the occurrence of all the levels up to the point of thresholding is deliberately mapped to zero (globally) without considering their local importance (connectivity). This effect is demonstrated in Fig. 10.

On the other hand, the proposed thresholding technique used to map a certain number of edge points at different edge intensity levels—Fig. 16 (*b*)—to zero instead of all the edge points corresponding to a few edge intensity levels. This is the reason why the proposed technique based on human visual characteristics gives a better result over the conventional technique.

7.　Discussion

Algorithms based on human psycho-visual phenomena are presented here for the automatic extraction of the significant edge points from those obtained by normal edge operators. Human visual characteristics are used to make the threshold selection procedure adaptive in order to eliminate the undesirable edge points. The results are found to be improved as compared to those obtained with standard thresholding techniques when unimodal, biomodal, multiple-valleyed, and flat-wide valleyed images are considered as input.

The task of gradient edge detectors was also replaced in a part of our study by some operators inherent to the thresholding procedure so that the computation time could be reduced without affecting the performance.

The background intensity computed over a larger window size makes the edges thinner. Splitting an image into sub-blocks (i.e. making the threshold selection procedure dynamic) on the other hand, enables one to detect more information.

The edge detection technique proposed in this paper does not require any human intervention. Although certain portions of the edges are found to be more than one pel width, these could be thinned out using standard edge-linking techniques. The probable application of the technique will be in the field of robot vision where the scope of human interaction is very limited.

REFERENCES

BROWN, E. L., and DEFFENBACHER, K., 1979, *Perception and Senses* (London: Oxford University Press).

BUCHSBAUM, G., 1980, *I.E.E.E. Trans. Biomed. Engng*, **27**, 237.

GONZALEZ, R. C., and WINTZ, P., 1977, *Digital Image Processing* (Mass., U.S.A.: Addison-Wesley).

HALL, E. L., 1979, *Computer Image Processing and Recognition* (New York: Academic Press).

KUNDU, M. K., and PAL, S. K., 1986, *Pattern Recogn. Lett.*, **4**, 433.

NEVATIA, R., 1982, *Machine Perception*. (Englewood Cliffs, N.J.: Prentice Hall).

PAL, S. K., and MAJUMDER, D. D., 1986, *Fuzzy Mathematical Approach to Pattern Recognition* (New York: Wiley).

ROSENFELD, A., KAK, A. C., 1982, *Digital Picture Processing* (New York: Academic Press).

WEZKA, J. S., 1978, *Comput. Graphic Image Process.*, **7**, 259.

ZUIDEMA, P., et al., 1983, *I.E.E.E. Trans. Systems Man Cyber.*, **13**, 923.